Data Mine

# An OBS Array to Investigate Offshore Seismicity during the 2018 Kīlauea Eruption

XiaoZhuo Wei*[1], Yang Shen[1], Jacqueline Caplan-Auerbach[2], and Julia K. Morgan[3]

## Abstract

**On 3 May 2018, Kīlauea Volcano, one of the most active volcanoes in the world, entered a new eruptive phase because of a dike intrusion in the East Rift zone. One day later, an $M_w$ 6.9 earthquake, which was likely trigged by the dike intrusion, occurred in the submarine south flank of Kīlauea Volcano. In mid-July, an ocean-bottom seismometer (OBS) array consisting of 12 stations was deployed on the submarine south flank of Kīlauea Volcano to monitor the aftershocks and lava–water interaction near the ocean entry. Eleven OBSs were recovered in mid-September. Preliminary evaluation of the data reveals a large number of seismic and acoustic events, which provide a valuable dataset for understanding flank deformation and stability as well as lava–water interaction. Here, we introduce this dataset and document notable instrument malfunctions along with some initial seismic and acoustic observations.**

**Cite this article as** Wei, X. Z., Y. Shen, J. Caplan-Auerbach, and J. K. Morgan (2020). An OBS Array to Investigate Offshore Seismicity during the 2018 Kīlauea Eruption, *Seismol. Res. Lett.* **92**, 603–612, doi: 10.1785/0220200206.

## Introduction

The 2018 Kīlauea eruption was one of the most important eruptions observed for Kīlauea Volcano in the past 200 yr. The collapse of its caldera was the eighth caldera collapse event documented globally in history (Anderson *et al.*, 2019). The precursory activity that led to the 2018 eruption started in March, and the first fissure erupted in Leilani Estates on 3 May (Neal *et al.*, 2019). On 4 May, the dike intrusion in the East Rift zone, which resulted in the eruption, triggered an $M_w$ 6.9 earthquake with an epicenter located offshore (Chen *et al.*, 2019; Neal *et al.*, 2019). The coseismic rupture area was ~1000 km$^2$ on the décollement fault (Liu *et al.*, 2018). Large earthquakes also happened along the basal décollement fault near Kalapana in 1975 and 1989 (Klein *et al.*, 2001). However, of these events, only the 2018 earthquake was accompanied by intense magmatism and summit collapse.

The eruption provided an opportunity to address several important questions: What structures within the Kīlauea south flank were activated during the 2018 event, and what deformation did they accommodate? Specifically, how was seismicity distributed within or near the décollement? Were the thrust faults and boundary faults identified by previous studies (Morgan *et al.*, 2003) activated by the $M_w$ 6.9 earthquake and volcano eruption? Because the rupture area of the 2018 earthquake might be different from those of previous earthquakes, it is expected that some faults and regions that had not been seismically active before might have become activated this time. What were the pattern and sequence of seismicity following the $M_w$ 6.9 earthquake, particularly near the epicenter?

To answer these questions, a team of researchers and students deployed 12 short-period Scripps LC4x4 ocean-bottom seismometers (OBSs) on the submarine south flank of Kīlauea, from July to September 2018. The stations were named from KSFA to KSFL (Table 1), where KSF stands for Kīlauea south flank. This was the first OBS deployment on Kīlauea's submarine south flank. Previously, the Plume-Lithosphere Undersea Mantle Experiment (PLUME) OBSs were deployed off the Island of Hawai'i (Wolfe *et al.*, 2009), and two OBS arrays were deployed in the Lō'ihi Volcano area (Bryan and Cooper, 1995; Merz *et al.*, 2019). Morgan *et al.* (2003) conducted a multichannel seismic survey in the south flank region but deployed no OBSs.

The deployment was carried out between 10 July (Hawaii local time, used hereinafter unless specified) and 12 July onboard R/V Ka'imikai O Kanaloa during the cruise KOK1805. Eleven of the 12 OBSs, all but station KSFJ, were recovered between 15 and 16 September, onboard *R/V Marcus G. Langseth* during the cruise MGL1806. The OBS sites are shown in Figure 1. Each OBS had a three-channel geophone (EL1, EL2, ELZ) with the lower corner frequency around 5 Hz and a one-channel hydrophone (EDH), which was deployed in a free-fall manner. The locations of the OBSs on the seafloor

1. Graduate School of Oceanography, University of Rhode Island, Narragansett, Rhode Island, U.S.A.; 2. Geology Department, Western Washington University, Bellingham, Washington, U.S.A.; 3. Department of Earth, Environmental and Planetary Sciences, Rice University, Houston, Texas, U.S.A.

*Corresponding author: xiaozhuo_wei@uri.edu

TABLE 1
**Basic Information and Status of the Ocean-Bottom Seismometer (OBS) Stations**

| Station | Start (UTC) | End (UTC) | Latitude | Longitude | Depth (m) | Status |
|---|---|---|---|---|---|---|
| KSFA | 2018/07/10 | 2018/09/15 | 19.120199 | −155.338898 | 1540 | Worked |
| KSFB | 2018/07/10 | 2018/09/15 | 19.135799 | −155.163193 | 1811 | Worked |
| KSFC | – | – | – | – | – | Failed |
| KSFD | 2018/07/10 | 2018/09/16 | 19.263201 | −154.979706 | 2200 | Problematic |
| KSFE | 2018/07/10 | 2018/09/16 | 19.2526 | −154.886002 | 3100 | Worked |
| KSFF | 2018/07/10 | 2018/09/16 | 19.2321 | −154.871704 | 3300 | Worked |
| KSFG | 2018/07/11 | 2018/09/16 | 19.213499 | −154.849594 | 3800 | Worked |
| KSFH | 2018/07/11 | 2018/09/16 | 19.1945 | −154.826294 | 4800 | Problematic |
| KSFI | 2018/07/11 | 2018/09/16 | 19.252199 | −154.706696 | 5000 | Worked |
| KSFJ | – | – | – | – | – | Failed |
| KSFK | 2018/07/12 | 2018/09/16 | 19.468399 | −154.727295 | 2000 | Worked |
| KSFL | 2018/07/12 | 2018/09/16 | 19.530001 | −154.749802 | 700 | Problematic |

were determined by acoustic ranging during the deployment. All channels had a sampling rate of 200 Hz.

The array geometry was designed to have stations KSFA–KSFC to monitor the earthquakes along the western boundary of the mobile flank, stations KSFD–KSFI to monitor the décollement basal thrust microseismicity under the Outer Bench, and stations KSFJ–KSFL to not only better constrain earthquake locations in the lower East Rift zone but also record the acoustic signals of lava–water interaction near the ocean entry (Fig. 1). Particularly, stations KSFE–KSFH formed a linear subarray that can be used to image the basal thrust structures.

## Data Quality

After OBS recovery, the data were screened by the U.S. Navy, and a negligible amount of data (~7.5 hr total) was censored. Then the data were handed over to the Scripps Institute of Oceanography for data archiving preparation. The data were sent to the Incorporated Research Institutions for Seismology Data Management Center (IRIS DMC) for unrestricted data access, along with the network metadata, under network code Z6 (Caplan-Auerbach *et al.*, 2018) in July 2019.

Among the 11 recovered OBSs, station KSFC did not record any data. Thus, only 10 of the 12 OBSs yielded usable data (Fig. 1). Figure 2 shows an example of 30 min low noise-level raw data from station KSFE, showing frequent seismicity.

We calculated the average noise power density functions (PDFs) for the three OBS channels (Fig. 3) from all stations using Modular Utility for STAtistical kNowledge Gathering (MUSTANG) provided by IRIS (Casey *et al.*, 2018). We found that the PDFs for the three seismic components are similar. Data in the 10–20 Hz band have a PDF of −120 dB, comparable to previous OBS projects (Aderhold *et al.*, 2018; Lynner *et al.*, 2020) and the new high-noise model and new low-noise model (Peterson, 1993), which represents typical onshore station noise levels. There is, however, a "mesa-shaped" irregularity around 6 Hz on all three channels, which is the "6 Hz Noise" documented previously in, for example, the East Pacific Rise (Monigle *et al.*, 2009), Eastern North American Margin (ENAM, Aderhold *et al.*, 2018; Lynner *et al.*, 2020), and Plumbing Reservoirs of the Earth Under Santorini (PROTEUS) experiments (Aderhold *et al.*, 2018). Accompanying the "6 Hz Noise," sometimes there is another noise center around 13 Hz. These noise signals are observed on seismic channels of nearly every OBS of this array; they are absent from hydrophones, suggesting that the signals are not geological in nature. In addition, the very high values between −140 and −160 dB in the EL1 panel (Fig. 3) were caused by the "dead" EL1 component of station KSFH. A similar pattern can also be observed in EL2, which is due to the "dead" EL2 channel of station KSFG. Such "dead" channels could be caused by a cable or connector failure (J. Babcock, personal comm., 2019). Interestingly, the EL2 channel of station KSFG became functional after 12 days and 3 hr, during an $M_w$ 5.3 earthquake that happened at 2018-07-23T06:53:38.82 (UTC) and associated with minor collapses of the walls along the Kīlauea crater. It leads us to suspect that a loose connection in the sensor might have been "reset" by the earthquake. This anomaly in the EL2 panel is less prominent compared with the counterpart in the EL1 panel.

Apart from these issues, the ELZ component of station KSFD had a very small amplitude (hundreds to thousands times smaller) compared with the other two components of the same station and all components of nearby OBSs. This is abnormal because all channels of the OBSs should share

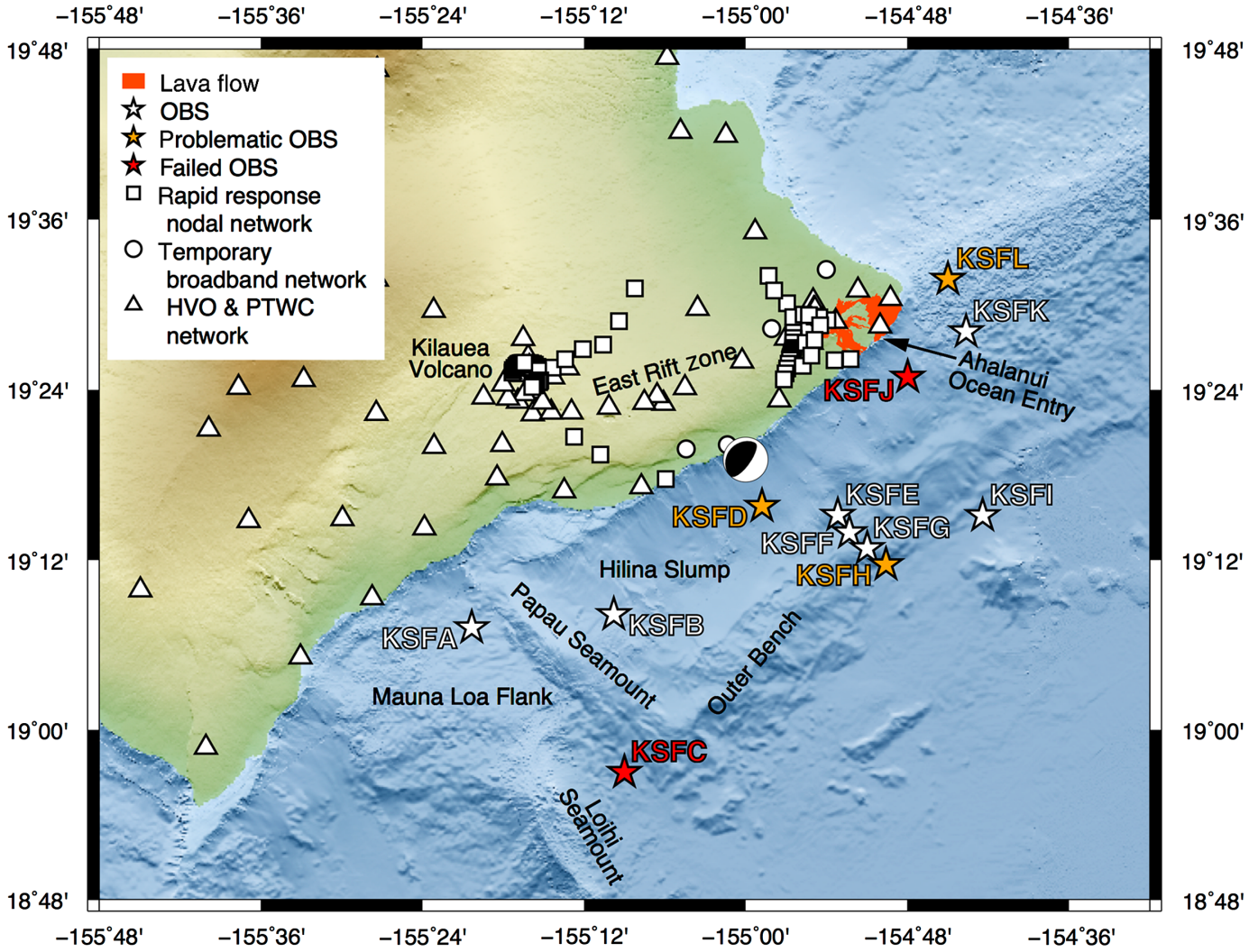


**Figure 1.** The distribution of the ocean-bottom seismometer (OBS) array and onshore seismic stations. Different symbols refer to different seismic networks. Different colors refer to different OBS station status; see the legend for details. Lava flow map is obtained from U.S. Gelogical Survey (Zoeller *et al.*, 2020). The Ahalanui Ocean Entry is marked by a black arrow. Some of the geographic features have been labeled on the map. The focal mechanism plot marks the epicenter and source mechanism of the $M_w$ 6.9 earthquake from National Earthquake Information Center's (NEIC) Centroid Moment Tensor (CMT) solution. The color version of this figure is available only in the electronic edition.

similar instrument responses. Besides, waveforms recorded on the ELZ channel of station KSFD consist of unusually high-frequency energy, distorting typical earthquake waveforms. The reason for this malfunction is not clear (J. Babcock, personal comm., 2019). A very similar problem also appears on the EL2 channel of station KSFL, although its amplitude is much closer to those of the other two components.

The loss of two stations (one unrecovered and one recorded no data) as well as the instrument malfunctions will, to some extent, adversely affect the original goals of this project. For example, the earthquake detection ability and location accuracy will not be as good as originally designed for the region around the southwest end of the south flank and Lō'ihi Volcano because station KSFC was a key station to monitor the seismicity in that region (Bryan and Cooper, 1995; Merz *et al.*, 2019). Similarly, both seismic and acoustic event detection ability and location accuracy in the ocean entry region deteriorate because of the missing of station KSFJ (Caplan-Auerbach *et al.*, 2019). The malfunction of channels on stations KSFD, KSFH, and KSFL can make it difficult to observe *S*-wave arrivals and prevent the usage of polarization based *P*- and *S*-wave decomposition, which is important for automated *S*-wave arrival picking (Ross *et al.*, 2016). Because OBS stations are usually noisier than land-based stations, sometimes the *S*-wave arrival is the only phase that can be picked for small earthquakes.

## Initial Observations and Results

### Seismic

The OBS array recorded a large number of earthquakes (Fig. 2). The majority of them are expected to have happened

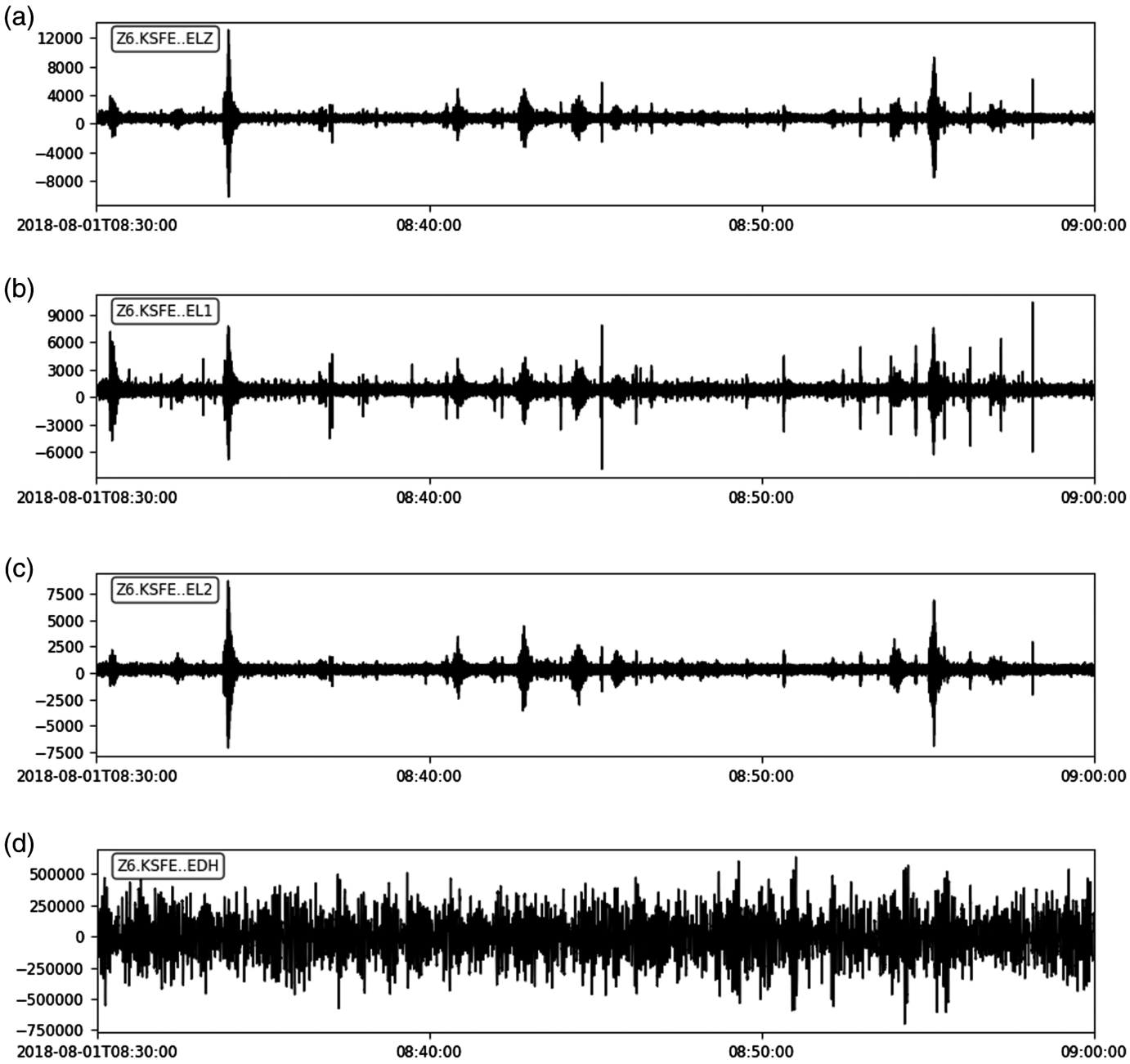


**Figure 2.** Thirty min raw data example from (a) ELZ, (b) EL1, (c) EL2, and (d) EDH channels of station KSFE, from 08:30 to 09:00 on 1 August 2018 (UTC). All units are in counts.

onshore, according to the onshore–offshore event ratio in the Hawaiian Volcano Observatory (HVO) catalog (B. Shiro, personal comm., 2020). A smaller but important number of events, not in the HVO catalog, occurred offshore. The HVO catalog has fewer than tens earthquakes under the submarine south flank during the OBS deployment period compared with more than 1000 events observed preliminarily by the OBS array.

Examples of an onshore event and two offshore events are shown in Figure 4. The first two earthquakes are selected from the HVO catalog. For these two events, both the *P*- and *S*-wave arrivals can be observed on most of the stations. The last event happened under the Outer Bench close to the linear subarray and cannot be found in the HVO catalog. This earthquake is expected to have a smaller magnitude because it was recorded only by the stations around the Outer Bench (Fig. 1), which is representative of the offshore events.

To detect the earthquakes, a recursive short-term average/long-term average (STA/LTA) algorithm (Withers *et al.*, 1998) is applied to the seismic records, after filtering them first between 8 and 12 Hz. The STA window length is 2 s, and the LTA window length is 30 s. An STA/LTA ratio larger than 3 is labeled as an event detection. After associating

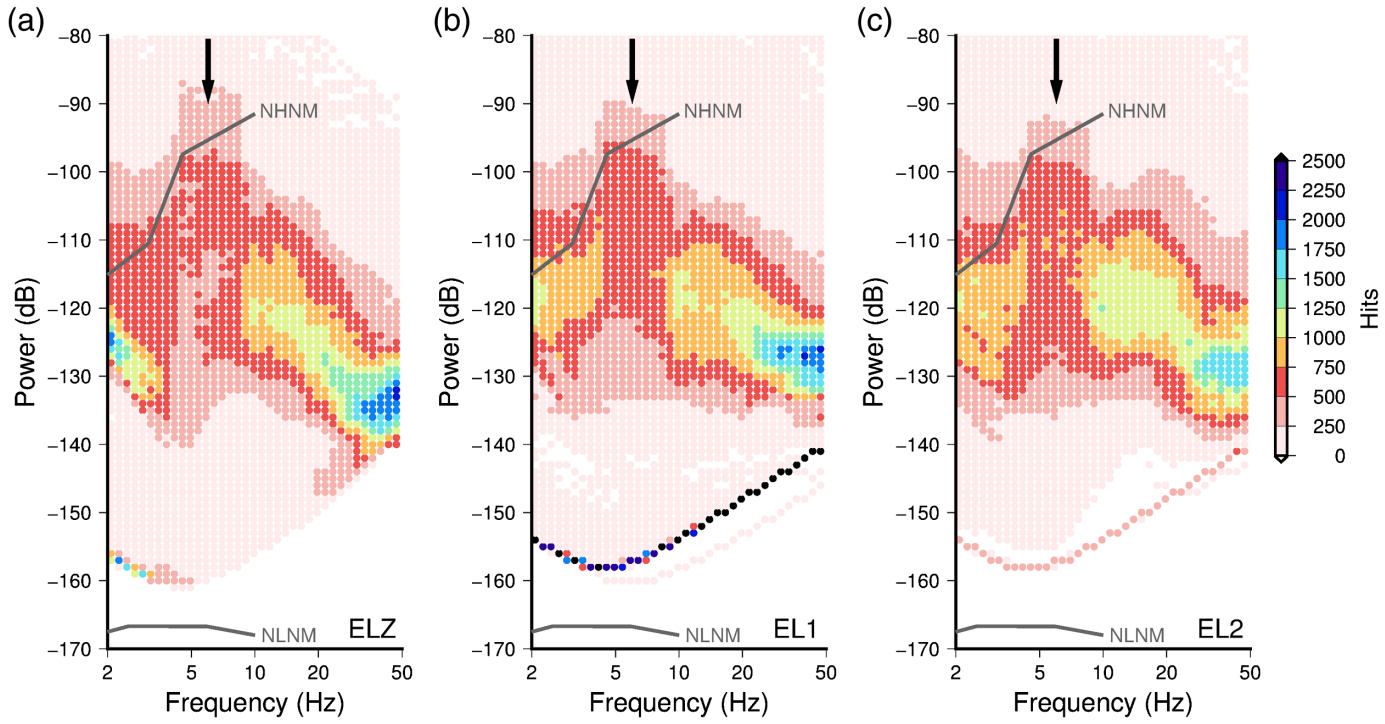


**Figure 3.** The average noise power density functions (PDFs) of the (a) ELZ, (b) EL1, and (c) EL2 channel. The black arrow indicates the noise peak at approximately 6 Hz. Colors from light to dark indicate data hit count (frequency distribution) from low to high. Two gray lines represents the new high-noise model (NHNM) and new low-noise model (NLNM), respectively (Peterson, 1993). The color version of this figure is available only in the electronic edition.

different station detections into different events, a kurtosis-based automated picker (Baillard *et al.*, 2014; Ross *et al.*, 2016) is applied to the waveforms to pick *P*- and *S*-wave arrival times. HYPOINVERSE-2000 v.1.40 (Klein, 2014) with a 1D velocity model simplified from Klein (1981) (Table 2) was used to locate the earthquakes. This is also the code used by the HVO to produce its earthquake catalog.

Our preliminary earthquake catalog consisting of 13,856 located events is shown in Figure 5 (Wei *et al.*, 2019). The OBS array is supplemented with the HVO permanent network (network code HV: U.S. Geological Survey [USGS] Hawaiian Volcano Observatory [HVO], 1956), the Pacific Tsunami Warning Center (PTWC) permanent network (network code PT: Pacific Tsunami Warning Center, 1965), a co-existing rapid response nodal array (network code Z1: Lin and Farrell, 2018), and a co-existing temporary broadband array (network code 4S: Johnson, 2018; Fig. 1). To focus on the offshore seismicity and events recorded by the OBS array, all the earthquakes included in this catalog needed to be detected by at least two OBS stations. For each station, the earthquake had to be detected on at least two channels for inclusion.

As expected, most earthquakes happened in the caldera region and along the East Rift zone, and there was a substantial number of earthquakes (~1300) located under the submarine south flank, especially around the four stations KSFE–KSFH. Some scattered seismicity in this preliminary catalog could be due to misidentification of arrivals in automated phase picking when events are clustered in time. Additional errors in locations could come from the use of a 1D velocity model in a place of large 3D velocity variations (Okubo *et al.*, 1997; Monteiller *et al.*, 2005; Park *et al.*, 2007, 2009; Lin *et al.*, 2014). We will closely inspect the scattered earthquakes as well as use a more accurate velocity model to confirm or remove scattered earthquakes in future studies.

Figure 6 shows a comparison of daily seismicity rates in the three subregions of Kīlauea Volcano between our initial catalog and the HVO catalog. The first and last days of OBS recording are removed to account for the incomplete array during instrument deployment and recovery that may bias event detection.

TABLE 2
**1D Velocity Model, Simplified from Klein (1981)**

| Depth (km) | $V_P$ (km/s) |
|---|---|
| −4.5 | 3.00 |
| 0.5 | 5.00 |
| 4.5 | 6.80 |
| 14.5 | 8.30 |

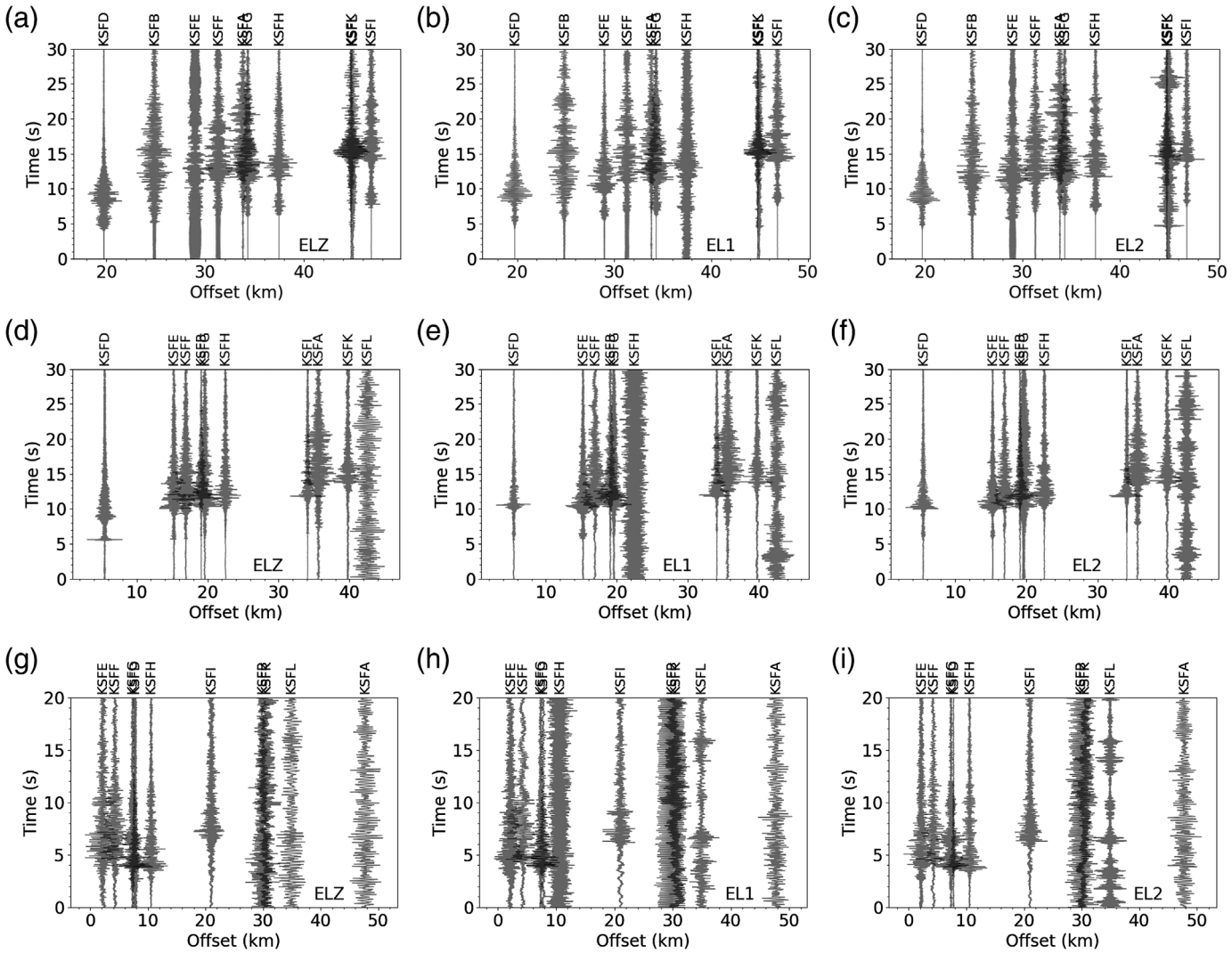


**Figure 4.** Three examples of recorded earthquakes, (a–c) one onshore and (d–f, g–i) two offshore. (a) The onshore $M_D$ 2.3 earthquake happened at 2018-09-06T10:36:24.45 (UTC), and the location is 19.359° N, 155.138° W at 7.1 km depth; (d–f) the first offshore $M_D$ 1.9 earthquake happened at 2018-09-06T18:25:39.81 (UTC), and the location is 19.254° N, 155.031° W at 39.13 km depth. Both origins are obtained from the Hawaiian Volcano Observatory (HVO) catalog. (g–i) The second offshore earthquake happened at 2018-08-14T23:11:32.02 (UTC), and the location is 19.2518° N, 154.9067° W at 15.82 km depth, selected from our preliminary catalog. Only the seismic channels of (a,d,g) ELZ, (b,e,h) EL1, and (c,f,i) EL2 are displayed. All traces are normalized to their own maximum to better show the data quality.

Despite some scattered seismicity and errors in location, we consider the daily seismicity rates within the subregions a robust statistical feature as defined by our event detection criteria. It is not surprising that our catalog contains fewer earthquakes near the caldera region than the HVO catalog because our selection criteria include detection on at least two OBSs. A substantial portion of the earthquakes in the caldera region have magnitudes below 2, making it difficult for the OBSs 30–40 km away to record these events. Nevertheless, the OBS array successfully captured the sharp drop of seismicity in the caldera region around 5 August 2018 (24 days after the beginning of OBS deployment on 10 July), marking the end of caldera collapse events (Neal *et al.*, 2019). On the other hand, our catalog contains more events during the OBS deployment period compared with the HVO catalog, not only in the submarine south flank but also in the East Rift zone region. The higher detection of events in the East Rift zone could be partially attributed to the additional nodal seismic stations there (Fig. 1) but not entirely because each event must be detected by at least two OBSs, and there were over 10 HVO stations near the rift. Most significant for this OBS dataset, the average daily event number in the south flank after 10 July changes from nearly zero in the HVO catalog to around 20 in our catalog. This demonstrates that the deployment of the OBS array can improve seismicity detection for

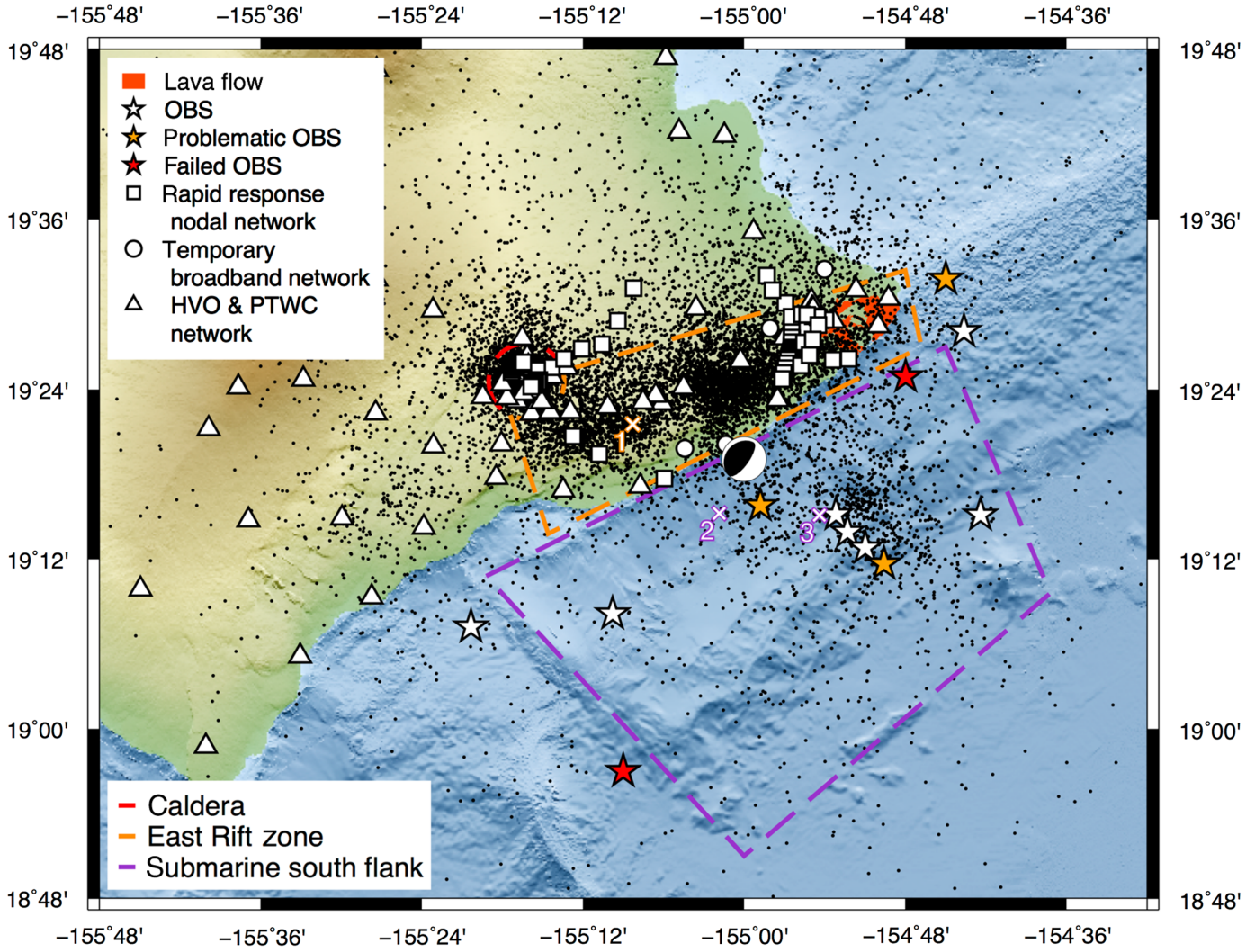


**Figure 5.** Earthquake locations (black dots) in the preliminary catalog obtained using the OBS array along with HVO and Pacific Tsunami Warning Center (PTWC) permanent stations and two other temporary seismic networks Z1 and 4S. The focal mechanism plot marks the location and source mechanism of the $M_w$ 6.9 earthquake, obtained from NEIC's CMT solution. Three dashed regions of red, dark orange, and dark purple mark the region of caldera, East Rift zone and submarine south flank used in Figure 6, respectively. The three crosses labeled with 1, 2, and 3 mark the location of the three earthquakes in Figure 4(a–c), (d–f), and (g–i), respectively. The color version of this figure is available only in the electronic edition.

the submarine south flank region greatly, as well as help monitor the onshore region, such as the East Rift zone of Kīlauea Volcano.

## Acoustic

Among the signals detected by the OBS array was activity at the ocean entry, where lava from the eruption poured into the sea. From 10 July, when the OBS deployment began, until the caldera collapse terminated in early August, there was at least one active ocean entry in the lower East Rift zone (Zoeller *et al.*, 2020). Most of the activity took place near Ahalanui (Fig. 1), although smaller entries were recorded all along the Puna coast. Activity at the coast was recorded on both seismic and hydroacoustic channels, but because the hydrophones were unaffected by 6 Hz noise, they render a clearer picture of ocean entry activity. Furthermore, compared with the seismometers, the hydrophones more clearly detected events such as lava–water explosions that took place in the water column, although many of these signals also coupled into the ground and were recorded on seismic channels.

Acoustic signals can be broadly divided into two categories: low-frequency (<10 Hz) signals that may be discrete or continuous and broadband (10–90 Hz) signals that are generally short in duration (a few seconds). A rapid onset of broadband signals at station KSFF on 11 July correlated with the onset of a new lava entry at Ahalanui, suggesting that these sounds are generated by lava–water interactions (Fig. 7). The source of the low-frequency signals is less certain but may correspond

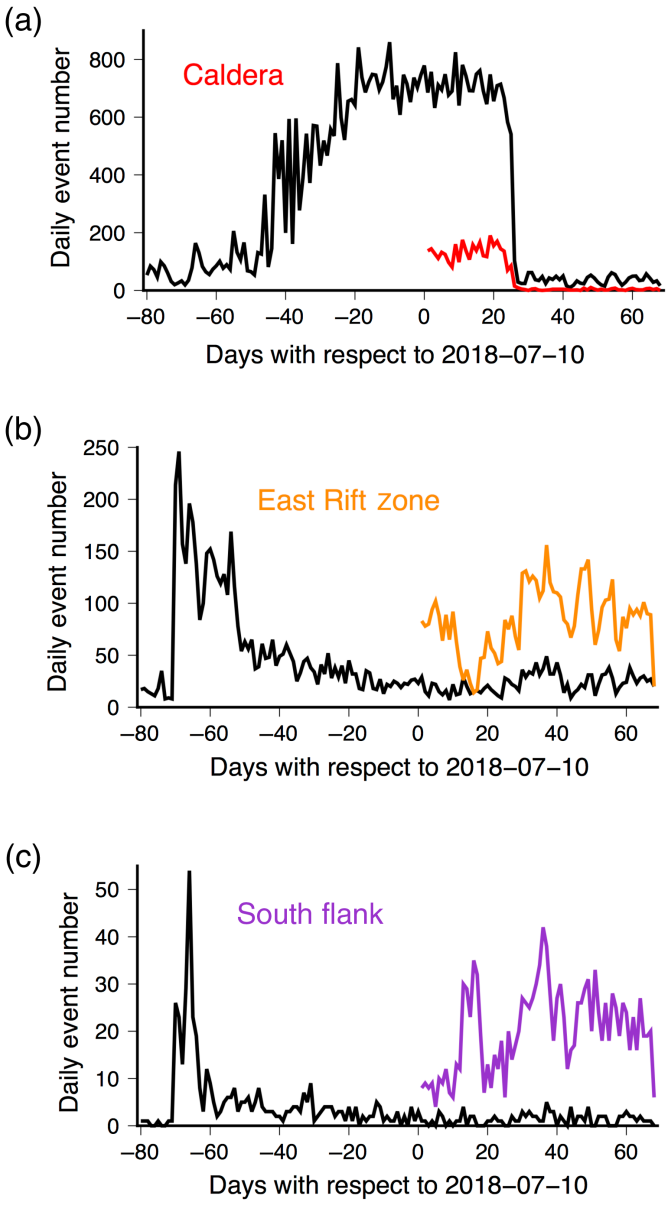


**Figure 6.** The daily earthquake numbers in our preliminary catalog of the three subregions, (a) the caldera, (b) East Rift zone, and (c) submarine south flank, represented by the red, dark orange, and dark purple curves, respectively. Black curves are the daily earthquake numbers from the HVO catalog. The color version of this figure is available only in the electronic edition.

to the flow of lava offshore, which has been well mapped by a recent survey (Soule *et al.*, 2019). That these signals are associated with the eruption is supported by a significant drop in broadband acoustic energy following the eruption's termination in early August.

Given that much of the lava erupted in the 2018 eruption was emplaced offshore, the acoustic data provide an important window into lava–water interactions and offshore emplacement of new material.


## Summary

To better understand the relationships between the 2018 Kīlauea eruption, the $M_w$ 6.9 earthquake, and the aftershock pattern under the volcano's south flank, 12 OBSs were deployed from 10 July to 16 September 2018. Ten of 11 recovered OBSs were functional, although three of them each had one problematic seismic channel. Nevertheless, preliminary analyses show that the OBS array recorded valuable data containing a great number of earthquakes, from both onshore to offshore, as well as acoustic signals of lava–water interaction. In particular, the OBS array enabled detection of more offshore earthquakes than in the HVO catalog, which only used onshore stations. The OBS dataset has been made publicly available at the IRIS DMC under network Z6 (Caplan-Auerbach *et al.*, 2018).


## Data and Resources

The recorded ocean-bottom seismometer (OBS) data are archived at Incorporated Research Institutions for Seismology Data Management Center (IRIS DMC) and can be accessed publicly under the network code Z6 (Caplan-Auerbach *et al.*, 2018). The Hawaiian Volcano Observatory (HVO) network used in this study can be accessed from IRIS DMC under the network code HV (U.S. Geological Survey [USGS] HVO, 1956). The Pacific Tsunami Warning Center (PTWC) network used in this study can be accessed from IRIS DMC under the network code PT (Pacific Tsunami Warning Center, 1965). The RAPID nodal array used in this study can be accessed from IRIS DMC under the network code Z1 (Lin and Farrell, 2018). The temporary broadband array used in this study can be accessed from IRIS DMC under the network code 4S (Johnson, 2018). The specifications of the Scripps LC4x4 OBS can be found at http://www.obsip.org/instruments/short-period/sio/specifications, and the specifications of the OBS be found at http://www.obsip.org/instruments/short-period/sio/response. The topography data are obtained through the Global Multi-Resolution Topography MapTool (Ryan *et al.*, 2009). The source mechanism of the 2018 $M_w$ 6.9 Kīlauea earthquake is obtained from USGS at https://earthquake.usgs.gov/earthquakes/eventpage/hv70116556. The Modular Utility for STAtistical kNowledge Gathering (MUSTANG) software is available online at http://service.iris.edu/mustang. All websites were last accessed in October 2020. Figures are plotted with Generic Mapping Tools (Wessel *et al.*, 2013) and ObsPy (Beyreuther *et al.*, 2010).


## Acknowledgments

The project design also benefited from conversations with Hawaiian Volcano Observatory (HVO) seismologists Paul Okubo and Brian Shiro and F.-C. Lin. The authors sincerely thank the crew members and the scientific party of cruise KOK1805 and MGL1806 along with the technicians from Scripps Institute of Oceanography for their help during the ocean-bottom seismometer (OBS) deployment and recovery. The first author thanks Jiarui Wu for the help with Figure 7. Constructive reviews from Brian Shiro and Kasey Aderhold helped improve this article. This study is supported by the Natioanl Science Foundation (NSF) RAPID Project Number 1840972 and NSF Grant Number 1949620.

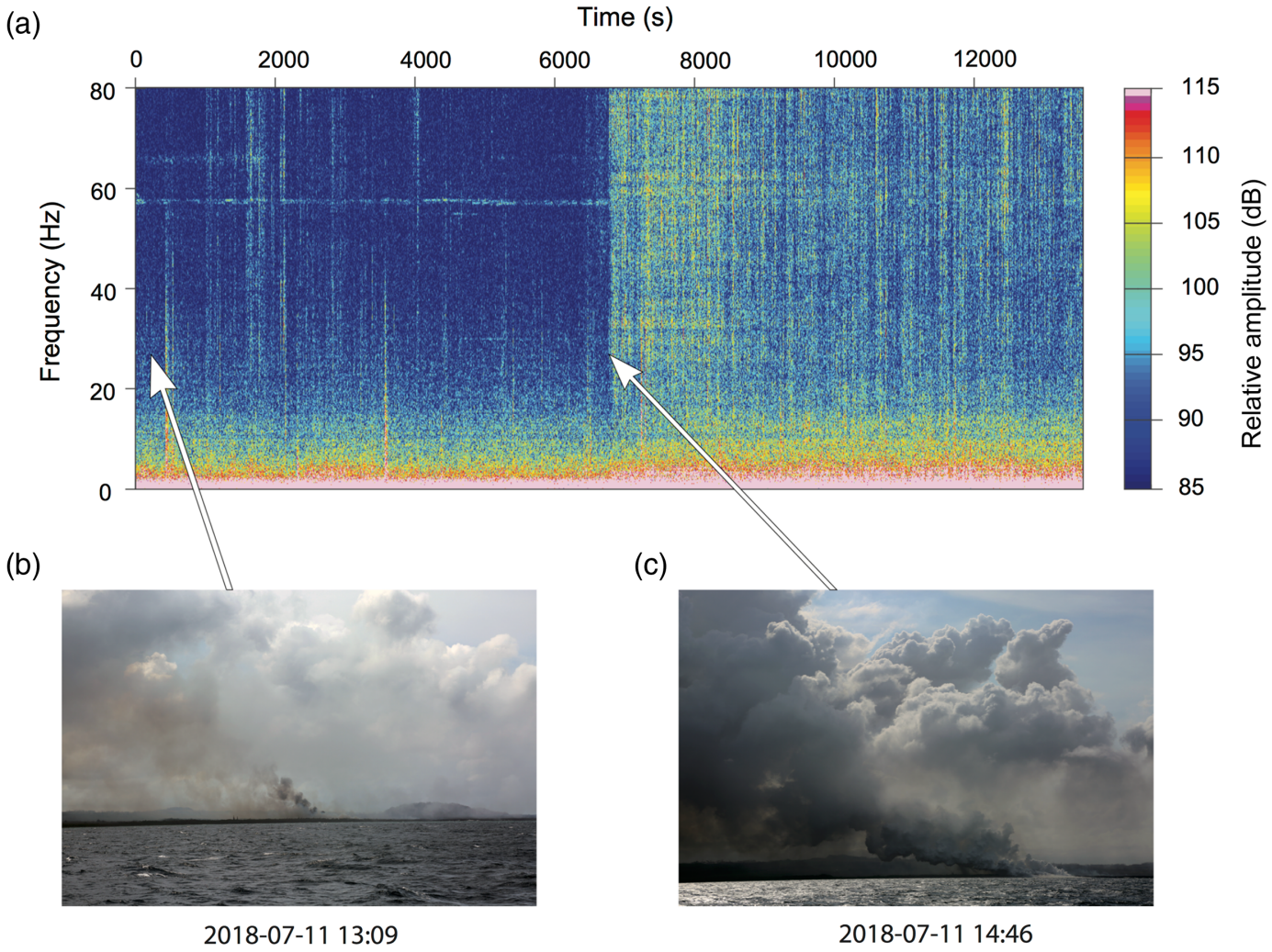


**Figure 7.** (a) Spectrogram recorded over a 3.75 hr period spanning the formation of the Ahalanui Ocean Entry on 11 July 2018. (b) The first photo shows the area at the beginning of the spectrogram, just before the lava's arrival at the coast. (c) The second photo shows the same view when lava reached the beach. Both photos were taken by Jacqueline Caplan-Auerbach on the ship during the deployment cruise. This time period correlates with an increase in acoustic amplitude (middle of the spectrogram) observed at station KSFF. The color version of this figure is available only in the electronic edition.

## References


Aderhold, K., A. Frassetto, G. Sharer, L. Keyson, and R. Woodward (2018). Ocean bottom seismometer data quality using MUSTANG, *2018 SSA Annual Meeting*, Miami, Florida, 14–17 May 2018.

Anderson, K. R., I. A. Johanson, M. R. Patrick, M. Gu, P. Segall, M. P. Poland, E. K. Montgomery-Brown, and A. Miklius (2019). Magma reservoir failure and the onset of caldera collapse at Kīlauea Volcano in 2018, *Science* **366,** no. 6470 doi: 10.1126/science.aaz1822.

Baillard, C., W. C. Crawford, V. Ballu, C. Hibert, and A. Mangeney (2014). An automatic kurtosis-based *P*-and *S*-phase picker designed for local seismic networks, *Bull. Seismol. Soc. Am.* **104,** no. 1, 394–409.

Beyreuther, M., R. Barsch, L. Krischer, T. Megies, Y. Behr, and J. Wassermann (2010). Obspy: A python toolbox for seismology, *Seismol. Res. Lett.* **81,** no. 3, 530–533.

Bryan, C., and P. Cooper (1995). Ocean-bottom seismometer observations of seismic activity at Loihi Seamount, Hawaii, *Mar. Geophys. Res.* **17,** no. 6, 485–501.

Caplan-Auerbach, J., J. K. Morgan, and Y. Shen (2018). OBS survey of Kilauea's submarine south flank following the May 4, 2018 M 6.9 earthquake and Lower East Rift Zone eruption, International Federation of Digital Seismograph Networks Z6 (2018–2018), doi: 10.7914/SN/Z6_2018.

Caplan-Auerbach, J., Y. Shen, J. Morgan, and S. Soule (2019). Hydroacoustic recordings of lava-water interactions and landslides during the 2018 eruption of Kilauea Volcano, *AGU Fall Meeting, 2019*, Paper Number V41A–01.

Casey, R., M. E. Templeton, G. Sharer, L. Keyson, B. R. Weertman, and T. Ahern (2018). Assuring the quality of IRIS data with MUSTANG, *Seismol. Res. Lett.* **89,** no. 2A, 630–639.

Chen, K., J. D. Smith, J.-P. Avouac, Z. Liu, Y. T. Song, and A. Gualandi (2019). Triggering of the Mw 7.2 Hawaii earthquake of 4 May 2018 by a dike intrusion, *Geophys. Res. Lett.* **46,** no. 5, 2503–2510.

Johnson, J. (2018). *UEA STAK Project*, National Geoscience Data Centre (NGDC), doi: 10.7914/SN/4S_2018.

Klein, F. W. (1981). A linear gradient crustal model for south Hawaii, *Bull. Seismol. Soc. Am.* **71,** no. 5, 1503–1510.

Klein, F. W., A. D. Frankel, C. S. Mueller, R. L. Wesson, and P. G. Okubo (2001). Seismic hazard in Hawaii: High rate of large earthquakes and probabilistic ground-motion maps, *Bull. Seismol. Soc. Am.* **91,** no. 3, 479–498.

Klein, R. (2014). User's guide to HYPOINVERSE-2000, a Fortran program to solve for earthquake locations and magnitudes, version 1.40, June 2014, *U.S. Geol. Surv. Open-File Rept. 02-171*.

Lin, F.-C., and J. Farrell (2018). Hawaii nodal rapid 2018 (ph5), *International Federation of Digital Seismograph Networks, Z1 (2018-2018)*, doi: 10.7914/SN/Z1_2018.

Lin, G., P. M. Shearer, R. S. Matoza, P. G. Okubo, and F. Amelung (2014). Three-dimensional seismic velocity structure of Mauna Loa and Kilauea volcanoes in Hawaii from local seismic tomography, *J. Geophys. Res.* **119,** no. 5, 4377–4392.

Liu, C., T. Lay, and X. Xiong (2018). Rupture in the 4 May 2018 Mw 6.9 earthquake seaward of the Kilauea east rift zone fissure eruption in Hawaii, *Geophys. Res. Lett.* **45,** no. 18, 9508–9515.

Lynner, C., H. J. A. Van Avendonk, A. Bécel, G. L. Christeson, B. Dugan, J. B. Gaherty, S. Harder, M. J. Hornbach, D. Lizarralde, M. D. Long, *et al.* (2020). The eastern North American margin community seismic experiment: An amphibious active-and passive-source dataset, *Seismol. Res. Lett.* **91,** no. 1, 533–540.

Merz, D., J. Caplan-Auerbach, and C. Thurber (2019). Seismicity and velocity structure of Lō'ihi submarine volcano and southeastern Hawai'i, *J. Geophys. Res.* **124,** no. 11, 11,380–11,393.

Monigle, P. W., D. R. Bohnenstiehl, M. Tolstoy, and F. Waldhauser (2009). Seismic tremor at the 9° 50' n East Pacific Rise eruption site, *Geochem. Geophys. Geosys.* **10,** no. 11, doi: 10.1029/2009GC002561.

Monteiller, V., J.-L. Got, J. Virieux, and P. Okubo (2005). An efficient algorithm for double-difference tomography and location in heterogeneous media, with an application to the Kilauea volcano, *J. Geophys. Res.* **110,** no. B12, doi: 10.1029/2004JB003466.

Morgan, J. K., G. F. Moore, and D. A. Clague (2003). Slope failure and volcanic spreading along the submarine south flank of Kilauea volcano, Hawaii, *J. Geophys. Res.* **108,** no. B9, doi: 10.1029/2003JB002411.

Neal, C. A., S. R. Brantley, L. Antolik, J. L. Babb, M. Burgess, K. Calles, M. Cappos, J. C. Chang, S. Conway, L. Desmither, *et al.* (2019). The 2018 rift eruption and summit collapse of Kīlauea Volcano, *Science* **363,** no. 6425, 367–374.

Okubo, P. G., H. M. Benz, and B. A. Chouet (1997). Imaging the crustal magma sources beneath Mauna Loa and Kilauea volcanoes, Hawaii, *Geology* **25,** no. 10, 867–870.

Pacific Tsunami Warning Center (1965). Pacific tsunami warning seismic system, International Federation of Digital Seismograph Networks (PT), doi: 10.7914/SN/PT.

Park, J., J. K. Morgan, C. A. Zelt, and P. G. Okubo (2009). Volcanotectonic implications of 3-D velocity structures derived from joint active and passive source tomography of the island of Hawaii, *J. Geophys. Res.* **114,** no. B9, doi: 10.1029/2008JB005929.

Park, J., J. K. Morgan, C. A. Zelt, P. G. Okubo, L. Peters, and N. Benesh (2007). Comparative velocity structure of active Hawaiian volcanoes from 3-D onshore-offshore seismic tomography, *Earth Planet. Sci. Lett.* **259,** nos. 3/4, 500–516.

Peterson, J. R. (1993). Observations and modeling of seismic background noise, *U.S. Geol. Surv. Open-File Rept. 93-322*.

Ross, Z., M. White, F. Vernon, and Y. Ben-Zion (2016). An improved algorithm for real-time *S*-wave picking with application to the (augmented) ANZA network in Southern California, *Bull. Seismol. Soc. Am.* **106,** no. 5, 2013–2022.

Ryan, W. B., S. M. Carbotte, J. O. Coplan, S. O'Hara, A. Melkonian, R. Arko, R. A. Weissel, V. Ferrini, A. Goodwillie, F. Nitsche, *et al.* (2009). Global multi-resolution topography synthesis, *Geochem. Geophys. Geosys.* **10,** no. 3, doi: 10.1029/2008GC002332.

Soule, A., E. Heffron, L. Gee, L. Mayer, N. A. Raineault, C. R. German, D. S. Lim, M. Zoeller, and C. Parcheta (2019). Mapping the lava deltas of the 2018 eruption of Kīlauea Volcano, *Oceanography* **32,** no. 1, 46–47.

U.S. Geological Survey (USGS) Hawaiian Volcano Observatory (HVO) (1956). Hawaiian volcano observatory network, *International Federation of Digital Seismograph Networks (HV)*, doi: 10.7914/SN/HV.

Wei, X., Y. Shen, J. Caplan-Auerbach, and J. Morgan (2019). Seismicity of the Kilauea submarine south flank following the 2018 eruption and Mw 6.9 earthquake, *AGU Fall Meeting, 2019*, Paper Number V41A–02.

Wessel, P., W. H. Smith, R. Scharroo, J. Luis, and F. Wobbe (2013). Generic Mapping Tools: Improved version released, *Eos Trans. AGU* **94,** no. 45, 409–410.

Withers, M., R. Aster, C. Young, J. Beiriger, M. Harris, S. Moore, and J. Trujillo (1998). A comparison of select trigger algorithms for automated global seismic phase and event detection, *Bull. Seismol. Soc. Am.* **88,** no. 1, 95–106.

Wolfe, C. J., S. C. Solomon, G. Laske, J. A. Collins, R. S. Detrick, J. A. Orcutt, D. Bercovici, and E. H. Hauri (2009). Mantle shear-wave velocity structure beneath the hawaiian hot spot, *Science* **326,** no. 5958, 1388–1390.

Zoeller, M., R. Perroy, R. Wessels, G. Fisher, J. Robinson, J. Bard, J. Peters, A. Mosbrucker, and C. Parcheta (2020). Geospatial database of the 2018 lower East Rift Zone eruption of Kīlauea volcano, Hawai'i, *U.S. Geol. Surv. Data Release*, doi: 10.5066/P9S7UQKQ.

**Manuscript received 28 May 2020**
**Published online 11 November 2020**